

Synthesis, Structural and Optical Characterization of Titanium Dioxide Doped by (Ce, Yb) Dedicated to Photonic Conversion

Zobair El Afia^{1,2,*}, Mohamed Youssef Messous², Mohammed Cherkaoui¹, and Mounia Tahri³

¹Laboratory of Materials, Electrochemistry, and Environment, Faculty of Sciences, University Ibn Tofail, 14000 Kenitra, Morocco

²Material Sciences Unit USM/DERS, National Center for Energy, Sciences and Nuclear Techniques-CNESTEN, B.P 1382 R.P 10001 Rabat, Morocco

³National Center for Energy, Sciences and Nuclear Techniques-CNESTEN-B.P 1382 R.P 10001 Rabat, Morocco

* **Corresponding author:**

email: zobair.elafia@gmail.com

Received: March 4, 2019

Accepted: September 4, 2019

DOI: 10.22146/ijc.43947

Abstract: The synthesis of TiO₂ co-doped by (Ce, Yb) rare earth couple has been realized. This couple of rare earth can convert a high-energy photon to two low energy photons to enhance the energy efficiency of silicon solar cells. The undoped, 2% Ce doped- and (2% Ce, 4% Yb) Codoped- Titanium oxide were prepared by the co-precipitation method. The Infrared spectroscopy FTIR-ATR analysis indicates a continuous visible absorption in the 750–400 cm⁻¹ region, confirming the formation of a titanium-oxygen bond. The X-Ray Diffraction characterization showed the dominance of the rutile crystalline phase with the presence of anatase one and the calculated crystallite size is between 7 to 13 nm. The X-Ray Fluorescence confirms the insertion of the dopants while the Inductively Coupled Plasma Mass Spectrometry ICP-MS showed the ratio 2 between Ce and Yb concentration. The thermogravimetric analysis indicated that Ce/Yb doped titanium was thermally stable. The absorption in the UV-visible (200 and 1000 nm) has been improved proportionally with the dopants.

Keywords: titanium dioxide; co-precipitation; rutile; anatase; photonic conversion

■ INTRODUCTION

Photovoltaic energy is one of the most important renewable energies, but this energy source has an efficiency limitation problem due to silicon used as a material for photon-electricity conversion. Recently, the Quantum Cutting process through which one high energy photon is converted into two near infrared ones attracted considerable attention. It can be adopted to minimize the energy loss by the thermalization of the charge carriers caused by the absorption of high-energy photons. Until here, some work has been done by combining Ytterbium (Yb) with other rare earth elements. In this paper, the preparation of Titanium dioxide, known as Titania, TiO₂, doped with the couple (Ce, Yb) was presented. It belongs to transparent semiconducting oxides (TCOs) class materials, which are simultaneously optically transparent

and electrically conductive. Titanium dioxide has great potential for a lot of applications such as photocatalytic treatment in wastewater, transparent devices in electronics and probes or light detectors and telecommunication transmitter devices [1-5].

There are different methods for the TiO₂ nanopowders preparation like thermal (ethanol thermal, hydrothermal and solvothermal) [6-12], dip coating [13], spin coating [14], electrochemical [15-17], chemical solvent [18], RF sputtering [19] and sol-gel [20-25]. The sol-gel process is one of the most successful techniques for preparing nanocrystalline TiO₂ due to its flexibility in fabrication, low cost, and low processing temperature. Due to the low absorption efficiency of commercial Silica-based cells, which are around 15%, titanium was used to improve the performance of these cells [26].

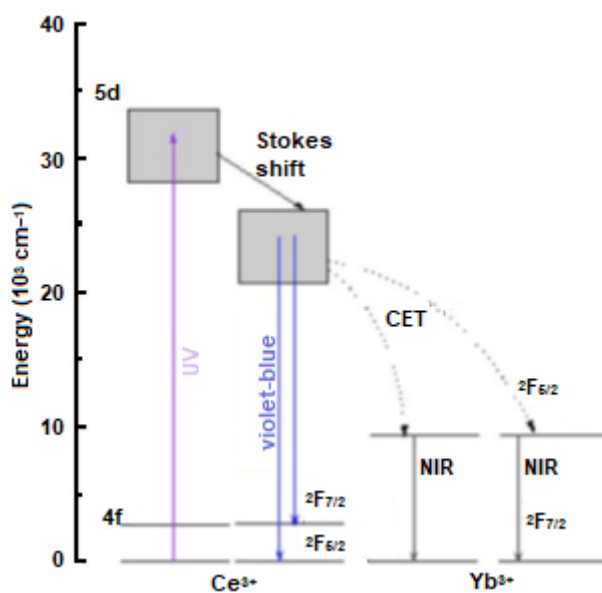


Fig 1. Schematic energy-level diagram of Ce/Yb cooperative energy transfer process from Ce^{3+} to Yb^{3+}

The synthesis of undoped and doped TiO_2 with Cerium and Ytterbium has been done by the co-precipitation method. This couple known for their exceptional optical properties attributed to down conversion [27-32], one ultraviolet/visible photon converted into two near infrared photons, which get absorbed by Si solar cells [33]. Indeed, the charge transfer (CT) follows the UV excitation of Ce^{3+} , from $\text{Ce}^{3+}:5d^1$ to $\text{Yb}^{3+}:^2F_{5/2}$ [34-37]. The NIR emission (976 nm and 1028 nm) occurs through the transition $\text{Yb}^{3+}:^2F_{5/2}$ to $\text{Yb}^{3+}:^2F_{7/2}$ Fig. 1 [38].

■ EXPERIMENTAL SECTION

Materials

The undoped and doped titanium dioxide, TiO_2 , was prepared using titanium trichloride solution 15% TiCl_3 (purity $\geq 99.95\%$), $\text{CeCl}_3 \cdot 7\text{H}_2\text{O}$ (99.9%) and $\text{YbCl}_3 \cdot 6\text{H}_2\text{O}$ (99.9%) precursors from Sigma-Aldrich. Fourier Transformed Infrared by Attenuated Total Reflection (ATR-FTIR) spectra was recorded in the 400–4000 cm^{-1} range on Perkin-Elmer spectrometer UATR two. Powder X-Ray diffraction (XRD) data was carried out with a D2-Phaser Diffractometer from Bruker. S2 Picofox–Bruker based on total reflection X-Ray Fluorescence (TXRF) used to provide a qualitative composition analysis when the

Inductively Coupled Plasma Mass Spectrometry ICP-MS exploited for quantitative one. For the thermogravimetric analysis, LABSYS EVO TGA was used in order to measure the amount of change in material as a function of increasing temperature.

Procedure

Undoped and doped TiO_2 preparation

For the preparation of undoped TiO_2 , 10 mL of titanium chloride was added in Erlenmeyer flask to 40 mL of distilled water. For the second sample TiO_2 (2% Ce) and the third TiO_2 (2% Ce, 4% Yb), 20 mg of CeCl_3 and (20 mg of CeCl_3 + 125 mg of YbCl_3) were added with TiCl_3 , respectively. The mixtures were prepared in an ice bath because the reaction was exothermic. The solutions were heated on a hot plate at 90 °C. The precipitates obtained dried at 110 °C in an oven for 24 h.

■ RESULTS AND DISCUSSION

X-Ray Diffraction Analysis (XRD)

The XRD diffraction spectrum for synthesis materials is illustrated in Fig. 2. The exhibited diffraction peaks for undoped titanium dioxide at 2θ values 25.05°, 47.5°, and 62.43° are attributed to anatase phase corresponding to crystal plans (101), (200), (204). Rutile peaks are found at 26.81°, 35.67°, 40.65°, 43.53°, 53.7°, and 56° corresponding to crystal plans (110), (101), (200), (210) and (022). For the Cerium doped titanium, Fig. 2 showed the anatase peaks at 2θ value 24.92°, 47.44°, and 62.43°. The rutile peaks appeared at $2\theta = 26.9^\circ, 35.6^\circ, 40.69^\circ, 43.44^\circ, 53.69^\circ, \text{ and } 56^\circ$. For the third sample, the spectrum showed anatase peaks at $2\theta = 25.23^\circ, 47.77^\circ, \text{ and } 62.49^\circ$, while the peaks at 26.96°, 35.65°, 40.93°, 43.5°, 53.87°, and 56° are attributed to rutile phase [39-40]. The additional intense peak at 31.2° in all samples is assigned to the reflection on (121) for the Brookite phase [36]. Average particle size D was estimated by using the Scherrer equation (Eq. (1)) [41], the results are presented in Table 1. The lattice parameters a , c and V for the undoped and doped titanium dioxide were calculated from the position (110) peak using the formulas in (Eq. (2)) [42]. Table 2 summarize all the calculated parameters. The introduction of Cerium and

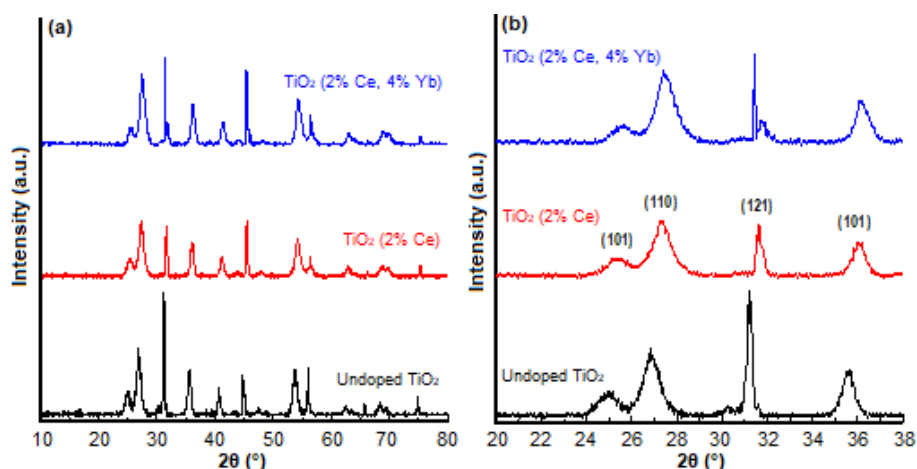


Fig 2. XRD of undoped and doped TiO₂: (a) total spectrum and (b) restricted spectrum

Table 1. Size crystallite D for the undoped TiO₂

Hkl	2θ (°)	Size (Å)
(101)	25.05	77.19
(103)	35.50	123.34
(121)	31.20	131.61

Table 2. Lattice parameters a, c, and V for different samples in plan (110)

	D (Å)	a (Å)	c (Å)	c/a	V (Å ³)
TiO ₂	88.39	3.85	6.68	1.73	86.10
TiO ₂ :2% Ce	76.75	3.84	6.65	1.73	85.26
TiO ₂ :2% Ce;4% Yb	79.22	3.83	6.64	1.73	84.70

Ytterbium atoms into TiO₂ shifted the position of the peak of TiO₂ (Fig. 2), reduced the grains size, and slightly decreased the lattice parameters Table 2.

$$D = \frac{K\lambda}{\beta \cos\theta} \quad (1)$$

$$a = \frac{\lambda}{\sqrt{3} \sin\theta} \quad \text{and} \quad c = \frac{\lambda}{\sin\theta} \quad (2)$$

where λ is the wavelength incident X-ray (= 1.549 Å); K: shape factor (= 0.9); β : Full-width at half maximum (FWHM) of the peak in the XRD patterns; θ : diffraction angle.

X-Ray Fluorescence Spectroscopy (XRF)

To study the elemental composition of TiO₂, qualitative analysis was performed by X-Ray Fluorescence (XRF) Spectroscopy analysis. The spectrum obtained is shown in Fig. 3. XRF pattern shows peaks at 4.51 keV and 4.93 keV corresponding to Ti, which is the major element present in the powder. The spectra corresponding to the doped TiO₂ shows Cerium at (4.80 keV; 5.26 keV; 5.61 keV; 6 keV and 6.30 keV) and Ytterbium at (7.18 keV and 8.40 keV) suggesting that

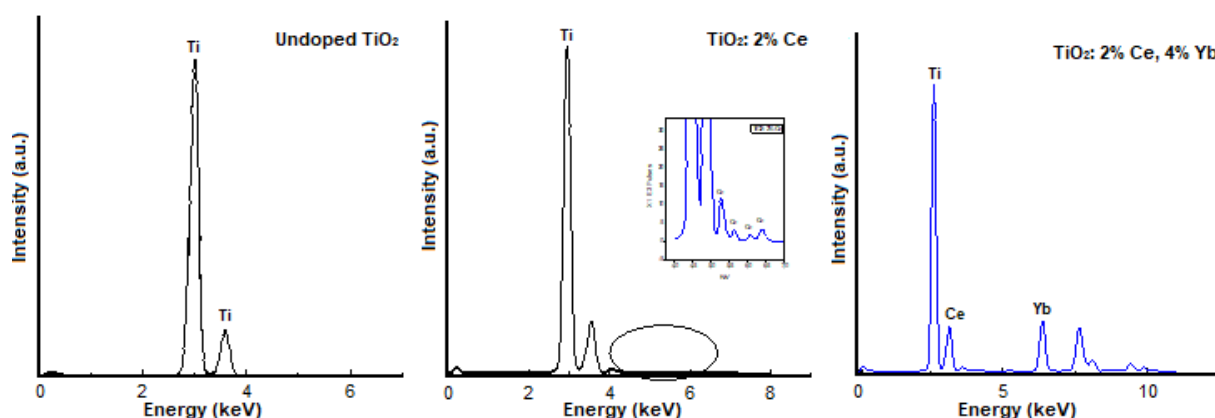


Fig 3. X-Ray fluorescence spectra of: undoped TiO₂; TiO₂ (2% Ce); TiO₂ (2% Ce, 4% Yb)

they were incorporated into the TiO₂ lattice. However, along with these elements, some impurities traces in the form of chlorine was observed.

Fourier Transform Infrared Spectroscopy (ATR-FTIR)

Fourier transform infrared spectroscopy was usually employed as an analytical technique to identify organic (in some cases inorganic) material. Fig. 4 shows the FTIR spectra for doped and undoped TiO₂. Water and alcohol content is marked as a broad peak in the region 3100–3500 cm⁻¹ and the narrow peak at 1620–1640 cm⁻¹.

The continuous absorption visible in all the samples in the region 750–400 cm⁻¹ are caused by the strong stretching vibrations of Ti-O and Ti-O-Ti bonds [43-44].

Inductively Coupled Plasma Mass spectroscopy ICP-MS

The concentrations obtained for sample (TiO₂: 2% Ce, 4% Yb) by ICP-MS technique are 39.89 ± 0.23 mg/g of ⁴⁷Ti, 4.20 ± 0.06 mg/g of ¹⁴⁰Ce and 8.74 ± 0.21 mg/g of ¹⁷²Yb. These data show a ratio of 2 between the concentrations of Ce and Yb and coincide with the quantity of the used precursors.

Thermogravimetric Analysis

The as-synthesized powder was measured for its thermal properties from room temperature to 900 °C. The TG analysis in Fig. 5 presents a weight loss of 8.5% between 25 to 198 °C, 4.5% in the range 198–600 °C and

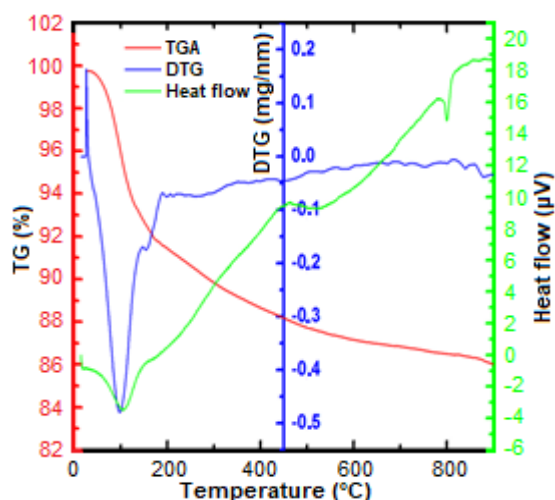


Fig 5. TGA/DTG curve of TiO₂ (2% Ce, 4% Yb)

non-appreciable loss is observed beyond 600 °C for (Ce, Yb) doped TiO₂ and an essentially constant mass (87% sample) has been found indicating the thermal stability of the sample. The mass loss until 198 °C attributed to complete dehydration of the powders. The DSC curve showed a broad peak around 799 °C which can be assigned anatase to rutile transformation [45].

UV-Vis Absorption

Fig. 6 shows the absorbance of the TiO₂ recorded between 200 and 1000 nm at room temperature. This absorbance is improved proportionally with the insertion of the dopants used; therefore, even small proportions of

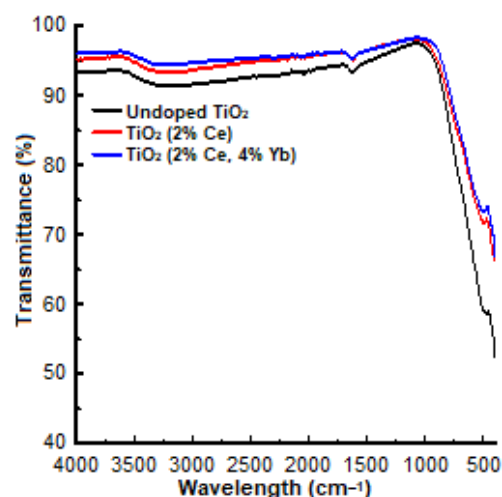


Fig 4. ATR-FTIR spectra of undoped TiO₂; TiO₂ (2% Ce) and TiO₂ (2% Ce, 4% Yb)

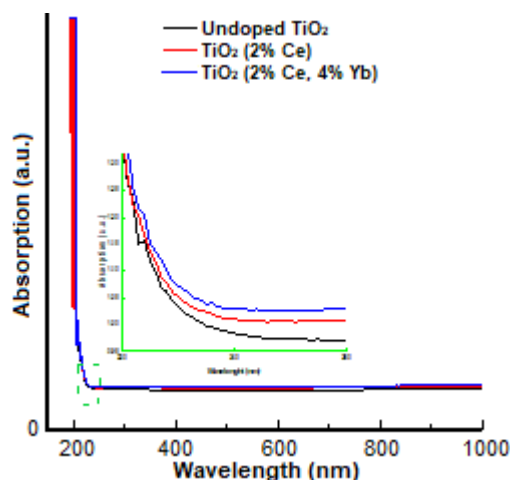


Fig 6. Absorption spectrum of undoped TiO₂; TiO₂ (2% Ce) and TiO₂ (2% Ce, 4% Yb)

the rare earth cerium and ytterbium enhance the optical properties of the TiO₂ remarkably.

■ CONCLUSION

The nano-powder titanium dioxide was synthesized by a simple co-precipitation method with an average crystalline size of 77 to 131 Å. The structure deduced from the XRD analysis shows that the nanoparticles are crystallized in the structures of rutile, which is the most dominant phase, also the presence of anatase and brookite phases. However, the introduction of the dopants decreases the size and lattice parameters of TiO₂ slightly. The elemental analysis by RFX shows the incorporation of Cerium and Ytterbium ions into the matrix, while the thermogravimetric analysis shows the transformation of the anatase structure into a rutile structure happened at high temperature between 700 and 800 °C and proved the thermal stability of the materials. Finally, the optical study by the UV-visible showed that the doping with the Ce and Yb rare earth increases the absorption of TiO₂ slightly, which allows it to be used for down-conversion in photovoltaic cells.

■ REFERENCES

- [1] Haider, A.J., AL-Anbari, R.H., Kadhim, G.R., and Salame, C.T., 2017, Exploring potential environmental applications of TiO₂ nanoparticles, *Energy Procedia*, 119, 332–345.
- [2] Gupta, K.K., Jassal, M., and Agrawal, A.K., 2008, Sol-gel derived titanium dioxide finishing of cotton fabric for self cleaning, *Indian J. Fibre Text. Res.*, 33, 443–450.
- [3] Afuyoni, M., Nashed, G., and Nasser, I.M., 2011, TiO₂ doped with SnO₂ and studying its structural and electrical properties, *Energy Procedia*, 6, 11–20.
- [4] Ray, S., and Lalman, J.A., 2016, Fabrication and characterization of an immobilized titanium dioxide (TiO₂) nanofiber photocatalyst, *Mater. Today-Proc.*, 3 (6), 1582–1591.
- [5] Banfield, J.R., and Zhang, H., 2001, Nanoparticles in the environment, *Rev. Mineral. Geochem.*, 44 (1), 1–58.
- [6] Feng, X., Wang, Q., Wang, G., and Qui, F., 2006, Preparation of nano-TiO₂ by ethanol-thermal method and its catalytic performance for synthesis of dibutyl carbonate by transesterification, *Chin. J. Catal.*, 27 (3), 195–196.
- [7] Askari, M.B., Banizi, Z.T., Soltani, S., and Seifi, M., 2018, Comparison of optical properties and photocatalytic behavior of TiO₂/MWCNT, CdS/MWCNT and TiO₂/CdS/MWCNT nanocomposites, *Optik*, 157, 230–239.
- [8] Wang, F., Shi, Z., Gong, F., Jiu, J., and Adachi, M., 2007, Morphology control of anatase TiO₂ by surfactant-assisted hydrothermal method, *Chin. J. Chem. Eng.*, 15 (5), 754–759.
- [9] Peng, F., Cai, L., Huang, L., Yu, H., and Wang, H., 2008, Preparation of nitrogen-doped titanium dioxide with visible-light photocatalytic activity using a facile hydrothermal method, *J. Phys. Chem. Solids*, 69 (7), 1657–1664.
- [10] Li, G., Chen, L., Dimitrijevic, N.M., and Gray, K.A., 2008, Visible light photocatalytic properties of anion-doped TiO₂ materials prepared from a molecular titanium precursor, *Chem. Phys. Lett.*, 451 (1-3), 75–79.
- [11] Zhao, X., Liu, M., and Zhu, Y., 2007, Fabrication of porous TiO₂ film via hydrothermal method and its photocatalytic performances, *Thin Solid Films*, 515 (18), 7127–7134.
- [12] Askari, M.B., Banizi, Z.T., Seifi, M., Dehaghi, S.B., and Veisi, P., 2017, Synthesis of TiO₂ nanoparticles and decorated multi-wall carbon nanotube (MWCNT) with anatase TiO₂ nanoparticles and study of optical properties and structural characterization of TiO₂/MWCNT nanocomposite, *Optik*, 149, 447–454.
- [13] Salehi, A., Mashhadi, H.A., Abravi, M.S., and Jafarian, H.R., 2015, An ultrasound assisted method on the formation of nanocrystalline fluorohydroxyapatite coatings on titanium scaffold by dip coating process, *Procedia Mater. Sci.*, 11, 137–141.

- [14] Mahadik, S.A., Pedraza, F., and Mahadik, S.S., 2016, Comparative studies on water repellent coatings prepared by spin coating and spray coating methods, *Prog. Org. Coat.*, 104, 217–222.
- [15] Karuppuchamy, S., Suzuki, N., Ito, S., and Endo, T., 2009, A novel one-step electrochemical method to obtain crystalline titanium dioxide films at low temperature, *Curr. Appl. Phys.*, 9 (1), 243–248.
- [16] Song, W., Wu, X., Qin, W., and Jiang, Z., 2007, TiO₂ films prepared by micro-plasma oxidation method for dye-sensitized solar cell, *Electrochim. Acta*, 53 (4), 1883–1889.
- [17] Anicai, L., Petica, A., Patroi, D., Marinescu, V., Prioteasa, P., and Costovici, S., 2015, Electrochemical synthesis of nanosized TiO₂ nanopowder involving choline chloride based ionic liquids, *Mater. Sci. Eng., B*, 199, 87–95.
- [18] Kim, B.H., Lee, J.Y., Choa, Y.H., Higuchi, M., and Mizutani, N., 2004, Preparation of TiO₂ thin film by liquid sprayed mist CVD method, *Mater. Sci. Eng., B*, 107 (3), 289–294.
- [19] Chernozem, R.V., Surmeneva, M.A., Krause, B., Baumbach, T., Ignatov, V.P., Tyurin, A.I., Loza, K., Epple, M., and Surmenev, R.A., 2017, Hybrid biocomposites based on titania nanotubes and a hydroxyapatite coating deposited by RF-magnetron sputtering: Surface topography, structure, and mechanical properties, *Appl. Surf. Sci.*, 426, 229–237.
- [20] Akpan, U.G., and Hameed, B.H., 2010, The advancements in sol-gel method of doped-TiO₂ photocatalysts, *Appl. Catal., A*, 375 (1), 1–11.
- [21] Crișan, M., Brăileanu, A., Răileanu, M., Zaharescu, M., Crișan, D., Drăgan, N., Anastasescu, M., Ianculescu, A., Nițoi, I., Marinescu, V.E., and Hodoroagea, S.M., 2008, Sol-gel S-doped TiO₂ materials for environmental protection, *J. Non-Cryst. Solids*, 354 (2-9), 705–711.
- [22] Shi, J.W., Zheng, J.T., Hu, Y., and Zhao, Y.C., 2007, Influence of Fe³⁺ and Ho³⁺ co-doping on the photocatalytic activity of TiO₂, *Mater. Chem. Phys.*, 106 (2-3), 247–249.
- [23] Saif, M., and Abdel-Mottaleb, M.S.A., 2007, Titanium dioxide nanomaterial doped with trivalent lanthanide ions of Tb, Eu and Sm: Preparation, characterization and potential applications, *Inorg. Chim. Acta*, 360 (9), 2863–2874.
- [24] Fan, X., Chen, X., Zhu, S., Li, Z., Yu, T., Ye, J., and Zou, Z., 2008, The structural, physical and photocatalytic properties of the mesoporous Cr-doped TiO₂, *J. Mol. Catal. A: Chem.*, 284 (1-2), 155–160.
- [25] Essalhi, Z., Hartiti, B., Lfakir, A., Siadat, M., and Thevenin, P., 2016, Optical properties of TiO₂ thin films prepared by sol gel method, *J. Mater. Environ. Sci.*, 7 (4), 1328–1333.
- [26] Zhang, H., Chen, J., and Guo, H., 2011, Efficient near-infrared quantum cutting by Ce³⁺-Yb³⁺ couple in GdBO₃ phosphors, *J. Rare Earths*, 29 (9), 822–825.
- [27] Reszczyńska, J., Esteban, D.A., Gazda, M., and Zaleska, A., 2014, Pr-doped TiO₂. The effect of metal content on photocatalytic activity, *Physicochem. Probl. Miner. Process.*, 50 (2), 515–524.
- [28] Kim, H.S., Li, Y.B., and Lee, S.W., 2006, Nd³⁺-doped TiO₂ nanoparticles prepared by sol-hydrothermal process, *Mater. Sci. Forum*, 510-511, 122–125.
- [29] Li, W., Wang, Y., Lin, H., Shah, S.I., Huang, C.P., Doren, D.J., Rykov, S.A., Chen, J.G., and Barteau, M.A., 2003, Band gap tailoring of Nd³⁺-doped TiO₂ nanoparticles, *Appl. Phys. Lett.*, 83 (20), 4143–4145.
- [30] Antić, Ž., Krsmanović, R.M., Nikolić, M.G., Marinović-Cincović, M., Mitrić, M., Polizzi, S., and Dramićanin, M.D., 2012, Multisite luminescence of rare earth doped TiO₂ anatase nanoparticles, *Mater. Chem. Phys.*, 135 (2-3), 1064–1069.
- [31] Chen, X., and Luo, W., 2010, Optical spectroscopy of rare earth ion-doped TiO₂ nanophosphors, *J. Nanosci. Nanotechnol.*, 10 (3), 1482–1494.
- [32] Mulwa, W.M., Ouma, C.N.M., Onani, M.O., and Dejene, F.B., 2016, Energetic, electronic and optical properties of lanthanide doped TiO₂: An ab initio LDA+U study, *J. Solid State Chem.*, 237, 129–137.
- [33] Qianqian, D., Feng, Q., Dan, W., Wei, X., Jianmin, C., Zhiguo, Z., and Wenwu, C., 2011, Quantum

- cutting mechanism in Tb^{3+} - Yb^{3+} co-doped oxyfluoride glass, *J. Appl. Phys.*, 110 (11), 113503.
- [34] Du, J., Wu, Q., Zhong, S., Gu, X., Liu, J., Guo, H., Zhang, W., Peng, H., and Zou, J., 2015, Effect of hydroxyl groups on hydrophilic and photocatalytic activities of rare earth doped titanium dioxide thin films, *J. Rare Earths*, 33 (2), 148–153.
- [35] Heng, C.L., Wang, T., Su, W.Y., Wu, H.C., Yin, P.G., and Finstad, T.G., 2016, Down-conversion luminescence from (Ce, Yb) co-doped oxygen-rich silicon oxides, *J. Appl. Phys.*, 119 (12), 123105.
- [36] van der Kolk, E., Ten Kate, O.M., Wiegman, J.W., Biner, D., and Krämer, K.W., 2011, Enhanced 1G_4 emission in $NaLaF_4: Pr^{3+}, Yb^{3+}$ and charge transfer in $NaLaF_4: Ce^{3+}, Yb^{3+}$ studied by Fourier transform luminescence spectroscopy, *Opt. Mater.*, 33 (7), 1024–1027.
- [37] Liu, Z., Li, J., Yang, L., Chen, Q., Chu, Y., and Dai, N., 2014, Efficient near infrared quantum cutting in Ce^{3+} - Yb^{3+} codoped glass for solar photovoltaic, *Sol. Energy Mater. Sol. Cells*, 122, 46–50.
- [38] Chen, D., Wang, Y., Yu, Y., Huang, P., and Weng, F., 2008, Quantum cutting down conversion by cooperative energy transfer from Ce^{3+} to Yb^{3+} in borate glasses, *J. Appl. Phys.*, 104 (11), 116105.
- [39] Haque, F.Z., Nandanwar, R., and Singh, P., 2017, Evaluating photodegradation properties of anatase and rutile TiO_2 nanoparticles for organic compounds, *Optik*, 128, 191–200.
- [40] Li, W., Liang, R., Hu, A., Huang, Z., and Zhou, Y.N., 2014, Generation of oxygen vacancies in visible light activated one-dimensional iodine TiO_2 photocatalysts, *RSC Adv.*, 4 (70), 36959–36966.
- [41] Binas, V.D., Sambani, K., Maggos, T., Katsanaki, A., and Kiriakidis, G., 2012, Synthesis and photocatalytic activity of Mn-doped TiO_2 nanostructured powders under UV and visible light, *Appl. Catal., B*, 113–114, 79–86.
- [42] Meddouri, M., Hammiche, L., Slimi, O., Djouadi, D., and Chelouche, A., 2016, Effect of cerium on structural and optical properties of ZnO aerogel synthesized in supercritical methanol, *Mater. Sci. Poland*, 34 (3), 659–664.
- [43] Tong, T., Zhang, J., Tian, B., Chen, E., and He, D., 2008, Preparation and characterization of anatase TiO_2 microspheres with porous frameworks via controlled hydrolysis of titanium alkoxide followed by hydrothermal treatment, *Mater. Lett.*, 62 (17–18), 2970–2972.
- [44] Zhou, L., Deng, J., Zhao, Y., Liu, W., An, L., and Chen, F., 2009, Preparation and characterization of N-I co-doped nanocrystal anatase TiO_2 with enhanced photocatalytic activity under visible-light irradiation, *Mater. Chem. Phys.*, 117 (2–3), 522–529.
- [45] Yodyingyong, S., Sae-Kung, C., Panijpan, B., Triampo, W., and Bull, D.T., 2011, Physicochemical properties of nanoparticles titania from alcohol burner calcinations, *Bull. Chem. Soc. Ethiop.*, 25 (2), 263–272.